J Comput Aided Mol Des (2012) 26:233–247
DOI 10.1007/s10822-011-9508-z

In silico inspired design and synthesis of a novel tubulin-binding anti-cancer drug: folate conjugated noscapine (Targetin)

Pradeep K. Naik · Manu Lopus · Ritu Aneja · Surya N. Vangapandu · Harish C. Joshi

Received: 26 June 2011 / Accepted: 1 December 2011 / Published online: 15 December 2011

Abstract Our screen for tubulin-binding small molecules that do not depolymerize bulk cellular microtubules, but based upon structural features of well known microtubule-depolymerizing colchicine and podophyllotoxin, revealed tubulin binding anti-cancer property of noscapine (Ye et al. in Proc Natl Acad Sci USA 95:2280–2286, 1998). Guided by molecular modelling calculations and structure–activity relationships we conjugated at C9 of noscapine, a folate group—a ligand for cellular folate receptor alpha (FRα). FRα is over-expressed on some solid tumours such as ovarian epithelial cancers. Molecular docking experiments predicted that a folate conjugated noscapine (Targetin) accommodated well inside the binding cavity (docking score −11.295 kcal/mol) at the interface between α- and β-tubulin. The bulky folate moiety of Targetin is extended toward lumen of microtubules. The binding free energy (ΔG_{bind}) computed based on molecular mechanics energy minimization was −221.01 kcal/mol that revealed favourable interaction of Targetin with the receptor. Chemical synthesis, tubulin-binding experiments, and anti-cancer activity in vitro corroborate fully well with the molecular modelling experiments. Targetin binds tubulin with a dissociation constant (K_d value) of 149 ± 3.0 μM and decreases the transition frequencies between growth and shortening phases of microtubule assembly dynamics at concentrations that do not alter the total polymer mass. Cancer cells in general were more sensitive to Targetin compared with the founding compound noscapine (IC_{50} in the range of 15–40 μM). Quite strikingly, ovarian cancer cells (SKOV3 and A2780), known to overexpress FRα, were much more sensitive to targetin (IC_{50} in the range of 0.3–1.5 μM).

Keywords Noscapine · Targetin · Folate-noscapine · Free energy of binding · Tubulin binding affinity · Microtubule dynamics · Anti-cancer activity

P. K. Naik (✉) · R. Aneja · S. N. Vangapandu · H. C. Joshi (✉)
Department of Cell Biology, Emory University School of Medicine, 615 Michael Street, Atlanta, GA 30322, USA
e-mail: pknaik1973@gmail.com; pnaik2@emory.edu

H. C. Joshi
e-mail: medhcj@emory.edu

M. Lopus
School of Biosciences and Bioengineering, Indian Institute of Technology Bombay, Powai, Mumbai 400076, India

Present Address:
M. Lopus
Department of Molecular, Cellular, and Developmental Biology, and the Neuroscience Research Institute, University of California, Santa Barbara, CA 93106, USA

Introduction

Microtubules are highly dynamic structures and their dynamic instability is responsible for many microtubule-dependent processes in cells such as cell motility, intracellular transport, maintenance of cellular morphology and cell division. Thus, any agent that changes the assembly or disassembly of microtubules can potentially prevent cell division by interfering with essential cellular functions. These agents, most notably colchicine, colcemid, nocodazole, paclitaxel and the vinca alkaloids have played seminal roles in probing the basic mechanisms of mitosis, inhibit cell proliferation and induce cell death [1–4]. Some of these compounds have been useful clinically in the management of a variety of neoplasms including ovarian cancer [5], breast cancer [6], lymphomas, lung cancer [7] and certain types of leukemia [8]. Mechanistically these drugs bind tubulin and prevent its

polymerization into microtubules (e.g. vinca alkaloids) or cause excessive polymerization (e.g. taxanes) resulting in altered microtubule polymer mass and indiscriminate cell death in normal and tumour cells [9]. However, drugs with more subtle effects even at high stoichiometric concentrations on microtubules that only modulate microtubule dynamics and do not alter total polymer mass may be clinically useful and be associated with fewer side effects. We discovered noscapine (an opium alkaloid widely used as an antitussive medicine) in a screen for such small molecules and demonstrated that noscapine: (1) binds stoichiometrically to tubulin, alters its conformation and assembly properties [10]; (2) interferes with microtubule dynamics both in vitro and in living cells [11, 12]; (3) blocks cell cycle progression at mitosis and causes apoptotic cell death in many cancer cell types [10, 13]; (4) possesses favourable pharmacokinetic property in vivo (clearance within ~10 h) [14–16]; (5) causes no significant side effects in tissues such as bone marrow, spleen, kidney, heart, liver, or small intestine and does not inhibit primary humoral immune responses in mice [11, 17].

Our research group has been involved in designing better and more effective derivatives of noscapine through structural modifications on the isoquinoline and dimethoxy benzyl furanone ring utilizing molecular modelling calculations followed by experimental evaluations [18–20]. Computational docking and competition studies of its derivative, 9-bromo-noscapine, point to binding with tubulin at a site overlapping with colchicine binding site [21]. The binding site is located at the interface between α- and β-tubulin and is large in volume (1,109.95 $Å^3$). The inner part of the binding cavity is mostly hydrophobic and the outer part is lined with both hydrophobic and hydrophilic amino acids. Moreover, the binding cavity is extended laterally through the inter-protofilament interface towards lumen of the microtubule. Therefore, there seems to be sufficient room available to fit larger functional groups. Furthermore, our initial efforts have been quite encouraging in that we have some more effective derivative of the lead compound, noscapine (K_d value is 152 ± 1 μM) by substituting halogen groups and nitro group at C9 position with higher binding affinity with tubulin (K_d value was decreased to 80, 54, 40, 22 μM by substituting F, Cl, Br, I and 86 μM by substituting NO_2 group) [18, 19]. Guided by molecular modelling calculations we recently designed an amino derivative, 9-amino-noscapine, that binds tubulin with higher affinity, dissociation constant (K_d) value of 14 ± 1 μM [20] than noscapine. However, there is no experimental work (such as site directed mutagenesis) has been done so far in deciphering which amino acids in the binding site play important role in establishing interaction with C9 position of noscapine. Encouraged by this result, here we sought to conjugate even bulkier group such as folate with the amino group because of two reasons: (1) the binding cavity is very large and it can accommodate a larger chemical moiety and (2) a particular type of folic acid receptor (FRα) is reported to be an over-expressed biomarker of certain metastatic aggressive cancer types such as the ovarian cancer [22, 23].

This study conceives folate-conjugated noscapine (also called Targetin, Fig. 1a) and evaluates specific interactions with tubulin based upon receptor-centric approaches. Receptor-centric methods such as molecular docking do not require experimental structure of the ligand and has become an essential and powerful platform for the discovery of new compounds and complement experimental approaches. Inspired by in silico results, we performed the chemical synthesis, tubulin binding properties, and anticancer activity of Targetin.

Materials and methods

Computational methodology

Protein preparation

The co-crystallized colchicine-tubulin complex structure (PDB ID: 1SA0, resolution 3.58 Å) [24] was used for

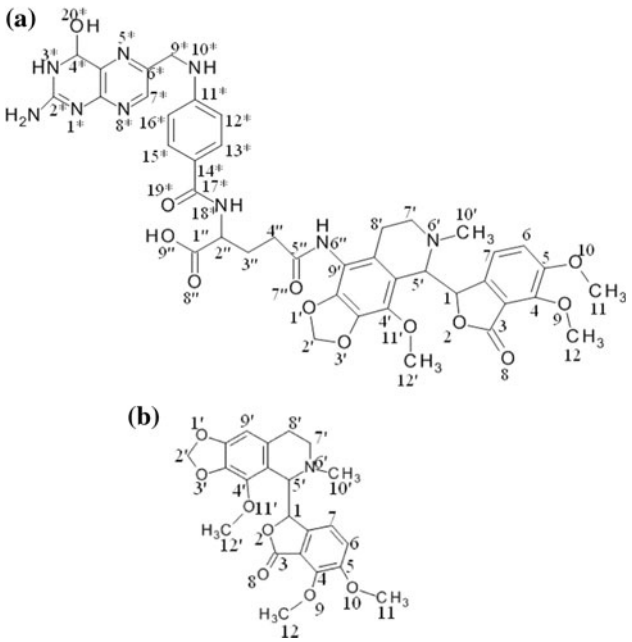

Fig. 1 Molecular structure of **a** Folate-noscapine (Targetin), and **b** Noscapine. **a** Targetin: IUPAC name: 2-[[4-[(2-amino-4-hydroxy-3,4-dihydropteridin-6-yl) methylamino] benzoyl]amino]-5-[[5-(4,5-dimethoxy-3-oxo-1H-isobenzofuran-1-yl)-4-methoxy-6-methyl-7,8-dihydro-5H-[1,3]dioxolo [4,5-g]isoquinolin-9-yl]amino]-5-oxo-pentanoic acid; Molecular formula: $C_{41}H_{43}N_9O_{12}$; Molecular weight: 853.83. Backbone atoms were numbered as per IUPAC nomenclature. **b** Noscapine: IUPAC name: 4,5-dimethoxy-3-oxo-(4-methoxy-6-methyl-7,8-dihydro-5H-[1,3]dioxolo[4,5-g]isoquinolin-9-yl)-1H-isobenzofuranone; Molecular formula: C19H17NO7; Molecular weight: 371.34. Backbone atoms were numbered as per IUPAC nomenclature

molecular docking and rescoring. There are certain amino acids which are missing in the co-crystallized structure but are not at close proximity to noscapinoid binding site. We retained a complex of colchicine-tubulin consisting of only 'A' and 'B' chains. The multi step Schrödinger's protein preparation wizard (PPrep) was used for the final preparation of protein. Missing hydrogen atoms were added to the structure automatically via the Maestro interface (version 8.5, Schrödinger) leaving no lone pair and using an explicit all atom model. All the water molecules were removed from the complex and optimized the hydrogen bond network using PPrep wizard. The complex obtained was energy minimized using OPLS 2005 force field with Polak-Ribiere Conjugate Gradient (PRCG) algorithm. The minimization was stopped either after 5,000 steps or after the energy gradient converged below 0.001 kcal/mol.

Ligand preparation

Molecular structures of both Targetin and noscapine were built using molecular builder of Maestro (version 8.5, Schrödinger). Both structures were energy minimized using Macromodel (version 9.1, Schrödinger) and MMFFs force field with PRCG algorithm (1000 steps of minimization and energy gradient of 0.001). Each structure was assigned an appropriate bond order using Ligprep (version 2.4, Schrödinger) and 32 (default value) conformations were generated for both Targetin and noscapine with correct chirality.

Ligand docking

We have adapted blind docking approach to predict the probable site of interaction of Targetin with the α- and β-tubulin complex. Different binding sites were predicted using SiteMap (version 2.4, Schrödinger), out of which only the top ranked five binding sites were selected based on site-score and volume for docking study. The physicochemical properties of these binding sites are included in Table 1. The receptor-grid files were generated at the centroid of each predicted binding site using Glide (version 2.5, Schrödinger). A bounding box of size 14Å × 14Å × 14Å was defined in tubulin and centered on the mass center of each binding site in order to confine the mass center of the docked ligand. The larger enclosing box of size 20Å × 20Å × 20Å was also defined (which occupied all the atoms of the docked poses). The dimension of both bounding box and enclosing box was optimized from many initial trials. The scale factor of 0.4 for van der Waals radii was applied to atoms of protein with absolute partial charges less than or equal to 0.25. Both Targetin and noscapine were then docked into each predicted binding site using Glide XP (extra precision) docking and refined further by QPLD (quantum mechanical-polarized ligand docking). QPLD is an improved docking method that incorporates quantum mechanical and molecular mechanical (QM/MM) calculations. It replaces the partial charges on ligand-atoms (assigned initially by force field during Glide XP run) with charges derived from QM calculations of ligand in the field of the receptor for each ligand-receptor complex. The QM charges were calculated from the electrostatic potential energy surface of the ligand generated from a single-point calculation using 3-21G basis set with BLYP (Becke's exchange potential and Lee–Yang–Parr correlation functional) density function. These ligands with updated atomic charges were then redocked onto the binding site using Glide XP. The detailed algorithm of the Glide docking has been described previously [25, 26]. Briefly, Glide approximates a systematic search of positions, orientations, and conformations of the ligand in the receptor binding site using a series of hierarchical filters. The shape and the properties of the receptor are represented on a grid by several different sets of fields that provide progressively accurate scoring of the ligand pose. Out of the 5,000 poses, that were sampled initially through exhaustive search of the torsional minima, 800 poses per ligand were selected for energy minimization (conjugate gradients 1,000 steps). The 10 lowest-energy poses obtained

Table 1 Docking results (Glide XP) of Targetin and noscapine with respect to different binding sites predicted by SiteMap (Schrödinger Inc.)

Site ID	Site score	Volume (Å)^3	Exposure	Enclosure	Hydrophobic	Hydrophilic	Donor/acceptor	Glide XP score (kcal/mol)	
								Targetin	Noscapine
1	1.081	1,109.95	0.424	0.819	0.564	1.341	0.590	−11.128	−4.727
2	1.037	167.04	0.539	0.751	1.311	0.764	1.524	−9.670	−4.075
3	1.028	598.88	0.586	0.701	0.345	0.870	1.762	−3.865	−3.436
4	0.903	134.46	0.462	0.725	0.340	0.348	0.787	−2.436	−2.375
5	0.837	98.44	0.523	0.680	0.120	0.376	1.197	−2.877	−2.316

Site 1, located at the interface between α- and β-tubulin is having better Glide score for both ligands. The physiochemical properties of the predicted binding sites are included. Predicted binding site 1 with higher values of site score, volume, enclosure, hydrophilicity and lower value of donor/acceptor ratio, in comparison to other binding sites reveals that this binding site is more appropriate for accommodating bulkier derivative like Targetin (consisting of many polar groups)

were subjected to post docking minimization (Monte Carlo sampling based on torsional minima and refining the orientation of side groups of ligand) and evaluated using a GlideScore function [27]. The choice of the best pose is made using a model energy score (Emodel) that combines the energy grid score, GlideScore, and the internal strain of the ligand.

Binding affinity prediction

A single best conformation for each ligand from QPLD was considered for rescoring based on two receptor-centric approaches, such as Prime MM-GBSA (molecular mechanics-generalized Born surface area) and Liaison (linear interaction approximation in implicit solvation), using the LSBD (ligand and structure based descriptors) application of the Schrödinger software package. A brief overview of these methodologies is described as follows.

Prime MM-GBSA calculation

Prime MM-GBSA calculates the free energy of binding between a ligand and a receptor. This method combines OPLS molecular mechanics energies (E_{MM}), surface generalized Born solvation model for polar solvation (G_{SGB}), and a nonpolar solvation term (G_{NP}) in order to calculate the total free energy of binding between the receptor and the ligand as follows. G_{NP} term comprises the nonpolar solvent accessible surface area and van der Waals interactions.

$$\Delta G_{\mathrm{bind}} = G_{\mathrm{complex}} - \left(G_{\mathrm{protein}} + G_{\mathrm{ligand}}\right) \quad (1)$$

$$G = E_{\mathrm{MM}} + G_{\mathrm{SGB}} + G_{\mathrm{NP}}$$

The docked poses were minimized using the local optimization feature in Prime (version 2.2, Schrödinger) and the energies were calculated using the OPLS 2005 force field and the GBSA continuum solvent model as described previously [28, 29]. During energy minimization, all the residues of the protein beyond 12 Å from the bound ligand were kept frozen.

Liaison calculations

Liaison (Liaison 4.0, Schrödinger) calculates various polar and non-polar energy components that are essential for the binding affinities between ligands and receptors by considering only two states: (1) free ligand in the solvent and (2) ligand bound to the solvated protein, using the surface generalized Born (SGB) implicit continuum solvation model [30]. Sampling technique such as hybrid Monte Carlo (HMC) was used for sampling the conformation of each ligand. A truncated Newton minimization (1,000 steps, OPLS 2005 force field) was first performed starting from the initial docked structures. The system was initially heated to 300 K in 5 ps and then subjected to a MD simulation for 15 ps. A residue-based cut off of 12 Å was set for the non-bonding interactions. The non-bonded pair list was updated every 10 fs. The time integration step of 1.0 fs and sampling of energies in every 10 steps was used. During the MD simulations, all the residues of the protein beyond 12 Å from the bound ligand were kept frozen. The time integration step of 1.0 fs and sampling of energies in every 10 steps was used as described previously [31]. The ensemble average energies for the ligand from bound and free form were obtained by performing MD simulations as per the receptor-ligand complex and subtracted to calculate the contribution of various energy terms in binding affinity of a ligand to a receptor as follows:

$$\begin{aligned}
\Delta G_{vdw} &= \left(\left\langle U^{b}_{vdw}\right\rangle - \left\langle U^{f}_{vdw}\right\rangle\right)\\
\Delta G_{coul} &= \left(\left\langle U^{b}_{coul}\right\rangle - \left\langle U^{f}_{coul}\right\rangle\right)\\
\Delta G_{rxn} &= \left(\left\langle U^{b}_{rxn}\right\rangle - \left\langle U^{f}_{rxn}\right\rangle\right)\\
\Delta G_{cav} &= \left(\left\langle U^{b}_{cav}\right\rangle - \left\langle U^{f}_{cav}\right\rangle\right)
\end{aligned} \quad (2)$$

Here $\langle\rangle$ represent the ensemble average, *b* represents the bound form of the ligand and *f* represents the free form of the ligand. U_{vdw}, U_{coul}, U_{rxn} and U_{cav} are the van der Waals, coulombic, reaction field and cavity energy terms in the SGB continuum solvent model. The cavity energy term U_{cav} is proportional to the exposed surface area of the ligand. Thus, the difference: $\left\langle U^{b}_{cav}\right\rangle - \left\langle U^{f}_{cav}\right\rangle$ measures the surface area lost by contact with the receptor. The contribution for net free energy of solvation comes from reaction field energy (U_{rxn}) and cavity energy (U_{cav}): $U_{SGB} = U_{rxn} + U_{cav}$. The cavity and reaction field energy terms implicitly take into account the van der Waals and the electrostatic interactions between the ligand and solvent. The electrostatic energy contribution was calculated as the sum of coulombic and reaction field energy terms.

Experimental methods

Chemical synthesis of Targetin

General ^{1}H NMR and ^{13}C NMR spectra were measured in CDCl3 on INOVA 400 NMR spectrometer. All proton NMR spectra were recorded at 400 MHz and were referenced with residual chloroform (7.27 ppm). All carbon NMR spectra were recorded at 100 MHz and were referenced with 77.27 ppm resonance of residual chloroform. Abbreviations for signal coupling are as follows: s, singlet; d, doublet; t, triplet; q, quartet; m, multiplet. Infrared spectra were recorded on sodium chloride discs on Mattson Genesis II FT-IR. High resolution mass spectra were collected on Thermo Finnigan LTQ-FT Hybrid mass spectrophotometer using

3-nitrobenzyl alcohol, in some cases with addition of LiI as a matrix. Melting points were determined using a Thomas Hoover melting point apparatus and were uncorrected. All reactions were conducted in oven-dried (125 °C) glassware under an atmosphere of dry argon. All common reagents and solvents were obtained from commercial suppliers and used without further purification unless otherwise indicated. Solvents were dried by standard methods. The reactions were monitored by thin layer chromatography (TLC) using silica gel 60 F254 (Merck) precoated aluminium sheets. Flash chromatography was carried out on standard grade silica gel (230–400 mesh).

Targetin was synthesized by coupling folic acid activated ester, NHS-folate, to 9-amino-noscapine. Synthesis of 9-amino-noscapine was discussed previously (Scheme 1) [20]. Briefly, noscapine (**1**) was dissolved in minimum amount of 48% hydrobromic acid and then cautiously added freshly prepared bromine water. The reaction mixture was stirred for 1 h at 25 °C and the pH was adjusted to 10 to afford 9-bromo-noscapine **(2)** in 82% yield. Refluxing of compound **2** in DMF with sodium azide and sodium iodide for 15 h produced 9-azido-noscapine (**3**) in quantitative yield. Reduction of 9-azido-noscapine with tin(II) chloride in the presence of thiophenol and triethylamine in THF for 2 h at 25 °C afforded 9-amino-noscapine (**4**) in 83% yield.

Synthesis of NHS-folate Briefly, Folic acid (10 mmol) was dissolved in dimethylsulfoxide (DMSO, 100 mL) in a flask. To this flask were added NHS (11 mmol) and dicyclohexylcarbodiimide (DCC, 11 mmol) sequentially under nitrogen atmosphere. The γ-carboxyl group is highly reactive compared to the tertiary carboxyl, and is further activated by using 1.1 molar excess of DCC to make an activated ester [32]. The reaction mixture was stirred overnight in dark at 25 °C. NMR spectral data do not suggest any intra-molecular reaction. Further evidence of chemical shifts of folate-NHS signals the folate backbone **5** and compound **6** and there was no peak at 12.36 ppm corresponding to the γ-carboxyl group on the spectra of folate-NHS compound **7** compared to that of folate **5** indicated that γ-carboxyl group of folate was conjugated with the *N*-hydroxy group of compound **6**. The insoluble and low molecular weight by-products were removed from the extraction mixture by filtering through a thick Celite pad. The folate-NHS product was further purified by loading onto a diethylaminoethyl (DEAE)-trisacryl anion exchange column and elucidated with an NH_4HCO_3 gradient. The folate-NHS was elucidated at 20 mM NH_4HCO_3, lyophilized and stored at −20 °C. The purity of the product was analyzed by silica gel thin-layer chromatography (TLC) using a solvent system composed of CH_2Cl_2/methanol (7/3, v/v) and the folate content of product was determined by using UV extinction at 363 nm. The yield was 84%.

Spectral details for characterization of NHS-folate:

IR: 2817(m), 2792(m), 2687(m), 1803(s), 1794(m), 1615(m), 1512(s), 1345(s), 1251(s), 1099(s), 935(w) cm-1; 1H NMR (CDCl3, 400 MHz), δ 11.21 (s, 1H), 8.42 (s, 1H), 8.12 (bs, 1H), 7.91 (d, 2H, $J = 6.3$ Hz), 6.63 (d, 2H, $J = 6.3$ Hz), 5.71 (bs, 1H), 4.73 (m, 1H), 4.45 (m, 2H), 4.1 (bs, 1H), 2.77 (t, 4H, $J = 2.3$ Hz), 2.31 (t, 2H, $J = 2.2$ Hz), 2.23 (m, 2H), 2.2 (bs, 1H), 2.0 (bs, 3H). 13C NMR (CDCl3, 100 MHz), δ 177.6 × 2, 168.8 × 2, 167.9, 163.3, 162.2, 151.9, 147.1 × 2, 142.8, 128.3 × 2, 121.7, 113.1 × 2, 72.1, 57.0 × 2, 26.2, 25.0, 21.8 × 2; HRMS (ESI): m/z calculated for C23H24N8O8 (M+1), 540.4912; experimentally determined, 541.2132 (M+1) (Scheme 2).

Conjugation of NHS-folate with amino-noscapine To a flask containing 9-amino-noscapine (10 mmol) dissolved in DMSO (100 mL) was added a solution of above-synthesized NHS-folate in DMSO under nitrogen atmosphere. The reaction mixture was stirred overnight in dark at 25 °C. The progression of the reaction was monitored by the depletion of primary amine measured by a ninhydrin assay (TLC system: 20% methanol in chloroform, plus 0.1% of acetic acid). The solvent DMSO was removed by evaporation *in vacuo* and the residue was dissolved in chloroform, filtered through a thick Celite pad to remove insoluble by-products. The filtrate was evaporated and the residue was purified by flash column chromatography (15% methanol in chloroform) to obtain Targetin (**8**) in 72%

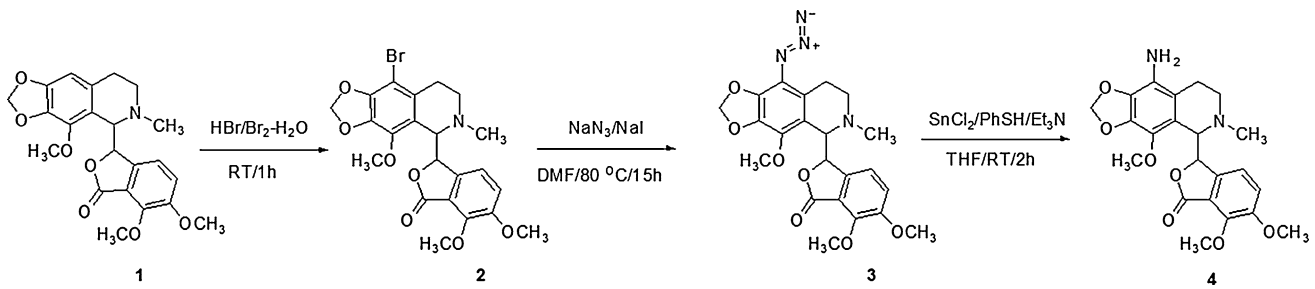

Scheme 1 Synthesis of 9-bromo-, 9-azido-, and 9-amino-noscapine derivatives

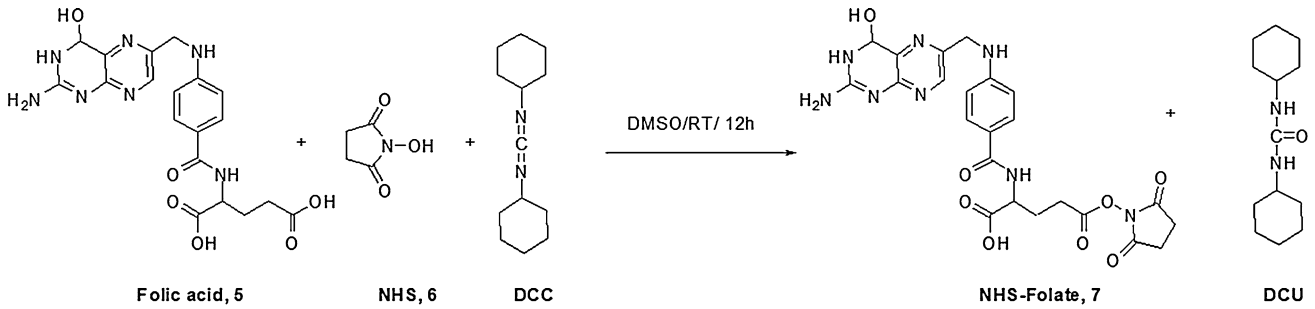

Scheme 2 Synthesis of folic acid activated ester (NHS-folate)

yield. When analyzed by silica-gel thin-layer chromatography, the product Targetin appeared as a single spot with a retention value of 0.85 (Scheme 3).

Spectral details for characterization of Targetin:

Yield: 72%; mp 123–124 °C; IR: 2945(m), 2800(m), 1759(s), 1612(m), 1500(s), 1443(s), 1263(s), 1091(s), 933(w) cm^{-1}; ^{1}H NMR ($CDCl_3$, 400 MHz), δ 11.44 (s, 1H), 8.64 (s, 1H), 8.14 (s, 1H), 8.11 (s, 1H), 7.66 (d, 1H, $J = 6.1$ Hz), 7.63 (d, 1H, $J = 6.1$ Hz), 7.27 (d, 1H, $J = 6.1$ Hz), 7.25 (d, 1H, $J = 6.1$ Hz), 6.95 (t, 1H, $J = 2.2$ Hz), 6.65 (d, 1H, $J = 4$ Hz), 5.99 (s, 4H), 5.53 (d, 2H, $J = 4$ Hz), 4.49 (bs, 1H), 3.94 (s, 3H), 3.86 (s, 3H), 3.79 (s, 3H), 3.34 (s, 4H), 2.56-2.45 (m, 7H), 2.40-2.25 (m, 4H); ^{13}C NMR (CDCl3, 100 MHz), δ 175.2, 171.8, 168.1, 167.5, 163.4, 162.1, 152.8, 149.7, 145.8 × 3, 143.9, 141.0, 138.3, 134.0, 129.1 × 2, 127.2, 120.9 × 2, 119.9, 117.8, 115.9, 114.8, 113.4 × 2, 90.5, 83.5, 82.8, 70.6, 58.5, 57.0 × 2, 56.5 × 3, 52.0, 36.4, 28.2, 27.0, 22.1; HRMS (ESI): m/z calculated for $C_{41}H_{43}N_9O_{12}$ (M+1), 853.8312; experimentally determined, 854.7522 (M+1).

Tubulin binding assay

Microtubule proteins (MTP) were isolated from goat brain in the presence of 1 M glutamate and 10% v/v DMSO by two polymerization-depolymerization cycles as described previously [33]. Tubulin was then purified using phosphocellulose chromatography [33, 34]. Tubulin concentration was determined by the method of Bradford using bovine serum albumin (BSA) as the standard. The purified tubulin was quickly frozen as drops in liquid nitrogen and stored at –80 °C until further use.

Binding of Targetin with tubulin was studied using a tryptophan-quenching assay as described previously [20, 35]. Briefly, Targetin (0–100 μM) was incubated with 2 μM tubulin in 25 mM PIPES, pH 6.8, 3 mM $MgSO_4$, and 1 mM EGTA for 45 min at 37 °C. The relative intrinsic fluorescence intensity of tubulin excited at 295 nm was then monitored in a JASCO FP-6500 spectrofluorometer (JASCO, Tokyo, Japan). The fluorescence emission intensity of Targetin at this excitation wavelength was negligible. A 0.3 cm path length cuvette was used to minimize the inner filter effects caused by the absorbance of these agents at higher concentration ranges. In addition, the inner filter effects were corrected using a formula $F_{\text{corrected}} = F_{\text{observed}} \cdot \text{antilog}\,[(A_{\text{ex}} + A_{\text{em}})/2]$, where A_{ex} is the absorbance at the excitation wavelength and A_{em} is the absorbance at the emission wavelength. The dissociation constant (K_d) was determined by the formula: $1/B = K_d/[\text{free ligand}] + 1$, where B is the fractional occupancy and [free ligand] is the concentration of free Targetin. The fractional occupancy (B) was determined by the formula $B = \Delta F/\Delta F_{\text{max}}$, where ΔF is the change in fluorescence intensity when tubulin and its ligand are in equilibrium and

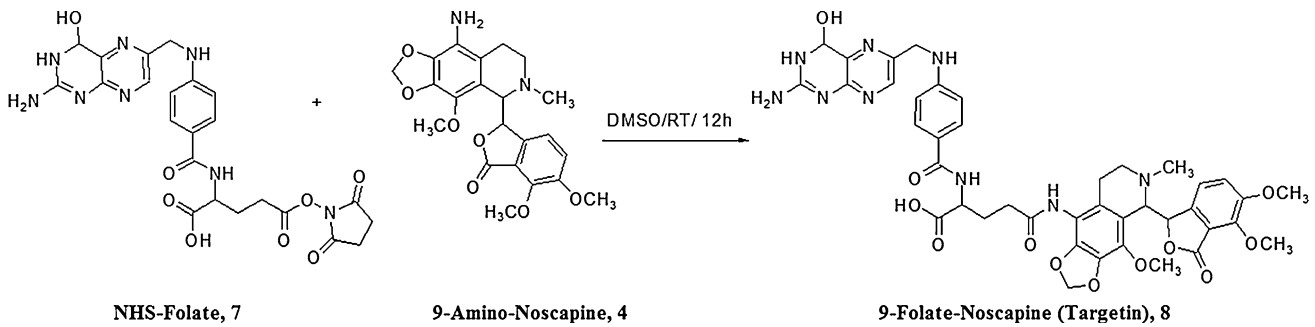

Scheme 3 Conjugation of NHS-folate with 9-amino-noscapine

ΔF_{max} is the value of maximum fluorescence change when tubulin is completely bound with its ligand. ΔF_{max} was calculated by plotting $1/\Delta F$ versus 1/ligand, using total ligand concentration as the first estimate of free ligand concentration.

Tubulin polymerization assay

Goat brain tubulin (1.0 mg/mL) was mixed with different concentrations of noscapine (25 or 100 μM) or Targetin (25 or 100 μM) at 0 °C in an assembly buffer (100 mM pipes at pH 6.8, 3 mM $MgS0_4$, 1 mM EGTA, 1 mM GTP, and 1 M sodium glutamate). Polymerization was initiated by raising the temperature to 37 °C in the water bath. The rate and extent of the polymerization reaction were monitored by light scattering at 550 nm, using a 0.3 cm path length cuvette in a JASCO FP-6500 spectrofluorometer (JASCO, Tokyo, Japan) for 30 min (samples were also removed for electron microscopic examination).

Microtubule dynamics analyses

For the analysis of microtubule dynamic instability we used cells stably transfected with green fluorescent protein-tagged α-tubulin (LLCPK-1α). The flat morphology of these cells enables us to visualize microtubule dynamics, individual microtubules are discernable in peripheral cell margins. Cells were treated with 5 and 10 μM Targetin for 60 min prior to imaging. Images were acquired at 6-s intervals with a Nikon Eclipse 300 microscope using a ×100, 1.3 numerical aperture objective lens and a micromax interline transfer cooled charge-coupled device camera (Roper Scientific) as previously described [11]. The positions of the microtubule ends were followed using the "track points" function of Metamorph software (Universal Imaging Corporation, Downington, PA) for all quantitative studies presented. A life history plot was generated for each microtubule and the phases of growth, shortening, and pause were selected. Only changes greater than 0.5 μm were considered for growth or shortening events. Changes less than 0.5 μm were included in the attenuated "pause" state. The duration, distance, rate of growth and shortening events were determined. The frequency of catastrophic events was determined by dividing the sum of the number of transitions from growth to shortening and from pause to shortening, by the sum of the duration of growth and pause. The frequency of rescue was determined by dividing the total sum of the number of transitions from shortening to growth and from shortening to pause by the time spent at shortening. Dynamicity is perhaps the best parameter to reflect overall dynamics and it was calculated by dividing the sum of the total length grown and shortened by the life span of the microtubule [11].

In vitro cell proliferation

The cell proliferation assay was performed in 96-well plates as described previously [12]. A panel of six cancer cell lines of different tissue origins such as lung (A549), colon (HCT116), prostate (DU145), breast (T47D), and ovarian (SK-OV3, 1A9) were considered for the assay. In brief, 2×10^3 cells were seeded in each well and incubated with gradient concentrations of Targetin and noscapine for 72 h. The cells were then fixed with 50% trichloroacetic acid and stained with 0.4% sulforhodamine B dissolved in 1% acetic acid. Cells were then washed with 1% acetic acid to remove excess (unbound) dye. The protein-bound dye was extracted with 10 mM Tris base to determine the optical density at 564 nm wavelength using a SPECTRAmax PLUS 384 microplate spectrophotometer (Molecular devices, Sunnyvale, CA).

Results and discussion

This study was inspired by our identification of position C9 on isoquinoline ring of noscapine that can accommodate substituents such as amino and azido groups [20] without interfering with tubulin interactions. (In fact, tubulin interactions can be enhanced substantially by modifications [18–20].) This encouraged us to explore if larger chemical moieties, such as small ligands for cellular receptors, can be accommodated at this position without compromising its anti-cancer effects. The primary motivation for this was to target cancer sub-types with known over expressed cell surface receptors in future. As a proof-of-concept, we initially chose a folate moiety primarily because a special type of its receptor (FRα) is over-expressed in certain cancer subtypes such as the ovarian epithelial carcinomas.

Computational study

The best way to understand the noscapinoid binding site is to obtain a co-crystal structure with tubulin, which is not yet possible so far. Alternatively, only one piece of experimental evidence (competition interaction of Br-noscapine with colchicine binding) is so far reported that revealed a binding site of noscapinoid at or near the colchicine binding site of tubulin [21]. We reported that Br-noscapine produced a competition of 66% with colchicine at a concentration of 100 μM. The extensive molecular modelling efforts reported previously revealed that most of the binding site amino acids for both noscapinoids and colchicine are almost identical (only few amino acids are uniquely involved in the binding of both the ligands with tubulin). Colchicine binding is biased more towards β-tubulin, whereas noscapinoids were interacted with both α- and β-tubulin. Since only one piece of

experimental evidence for binding of noscapinoid with tubulin is available and it will be experimentally difficult to realize the co-crystal structure of noscapinoid with tubulin due to unstability of tubulin structure, we adapted blind docking approaches to understand the mode of interactions of Targetin and noscapine with tubulin. Infact most of the

Table 2 Refinement of Glide XP docking poses of Targetin and noscapine with QPLD and their energy scores

Ligand	QPLD score (kcal/mol)	Glide energy (kcal/mol)	Glide E_{vdw} (kcal/mol)	Glide E_{coul} (kcal/mol)	Glide H_{bond} (kcal/mol)	Glide E_{model} (kcal/mol)
Targetin	−11.295	−61.599	−17.198	−44.401	−2.092	−72.598
Noscapine	−4.752	−24.363	−9.341	−15.022	−0.700	−26.439

QPLD generated more precise binding conformations of both lignads with increased binding affinity in comparison to standard Glide XP docking

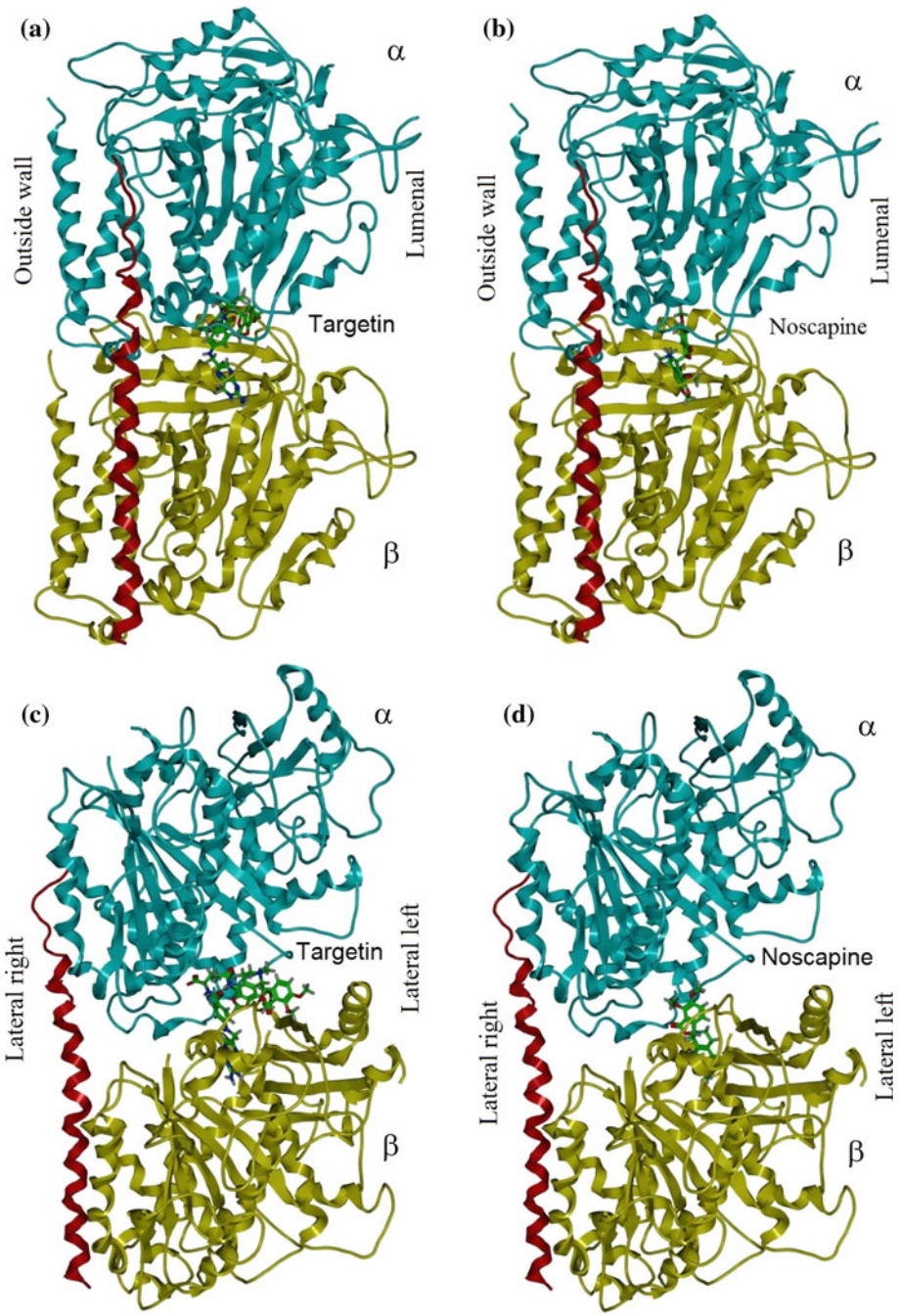

Fig. 2 Typical snapshots of Targetin (**a**, **c**) and noscapine (**b**, **d**) bound to tubulin at the interface between α- and *β*-tubulin from QPLD (quantum polarized ligand docking). In case of Targetin the folate moiety protrudes laterally through the inter-protofilament interface towards lumen of the microtubule (**c**), whereas the conjugated noscapine is biased towards the *β*-tubulin. Stathmin-like domain is represented in *red ribbon colour*

binding site amino acids elucidated from docked Targetin and noscapine in this manuscript also include the amino acids resolved from the Br-noscapine binding site, although a larger binding cavity has inspired that accommodated a larger derivative like Targetin. For an example the amino acids such as CYS B 241, ALA B 250, LYS B 254, LEU B 255, LYS B 352 and THR B 353 are involved in the interaction of both Br-noscapine, Targetin and Noscapine with tubulin.

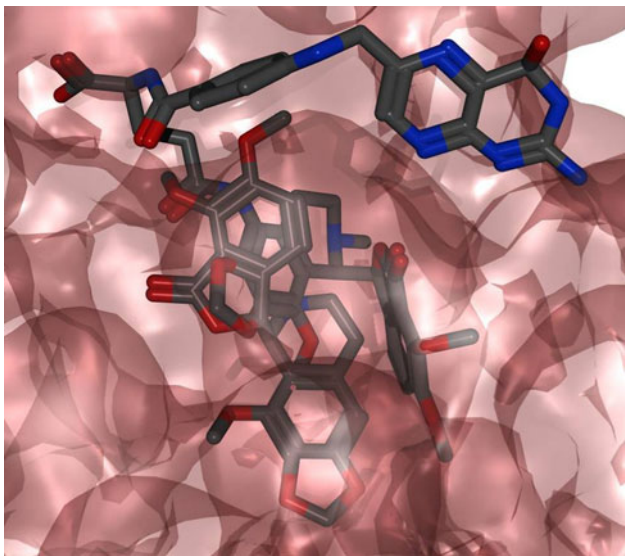

Fig. 3 Both Targetin and noscapine are well accommodated in the binding cavity of tubulin. At the outer side of the binding site the folate moiety of Targetin protrudes laterally towards the microtubule lumen. The conjugated noscapine of Targetin buried inside the binding cavity (image is presented as translucent to visualize the burried hidden parts). The noscapine molecule alone is also docked inside the binding cavity and is overlaid with the conjugated noscapine of Targetin

Both the ligands were docked into the predicted binding sites using flexible docking procedure in Glide XP. Five different binding sites with different site scores were predicted with different physiochemical properties (Table 1). Predicted binding site 1 with higher values of site score, volume, enclosure, hydrophilicity and lower value of donor/acceptor ratio, in comparison to other binding sites reveals that this binding site is more appropriate for accommodating bulkier derivative like Targetin (consisting of many polar groups). The docking results also revealed that both Targetin and noscapine bind with better docking score (−11.128 and −4.727 kcal/mol) and Emodel energy (−90.643 and −25.463 kcal/mol) with predicted binding site 1, located at the interface between α- and β-tubulin (Table 1). Targetin shares higher values of electrostatic interaction (E_{coul}) and van der Waals interaction (E_{vdw}) energies predicted by Glide-XP (Table 2) because of the polar and non polar interactions of substituted distal folate group with the binding site amino acids.

Obtaining accurate structural information on the binding pose of a ligand into a binding site is essential to the design of optimized lead compounds in computer-aided drug

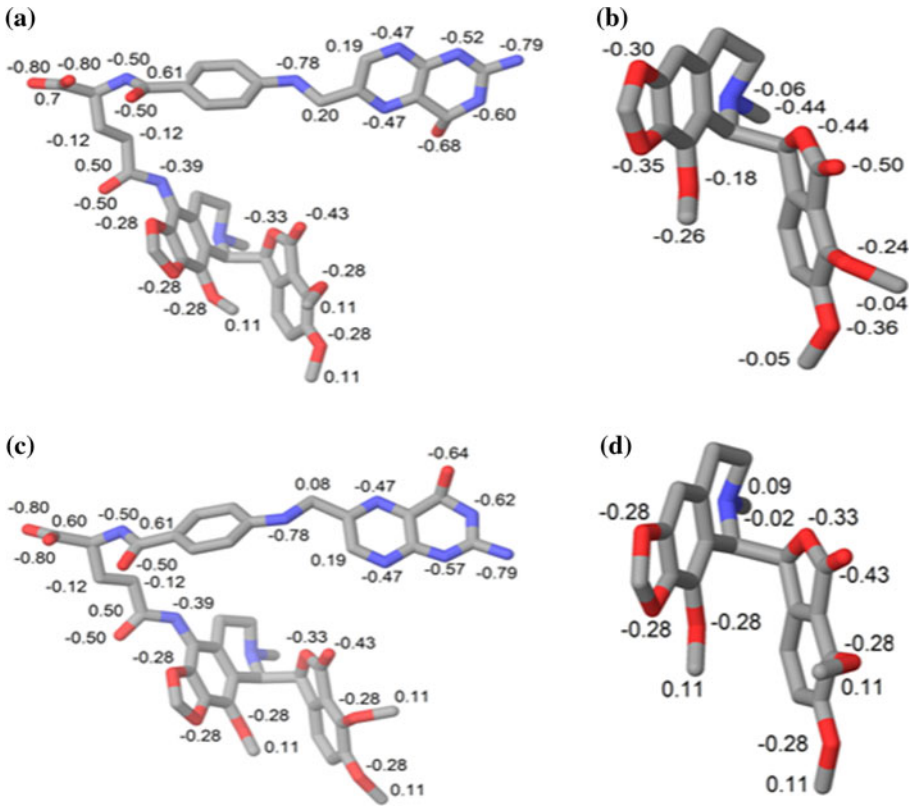

Fig. 4 Comparison between quantum mechanical charges (**a**, **b**), and MMFFs force field charges (**c**, **d**) for Targetin and noscapine from standard Glide docking and QPLD. Significant changes in partial charges of both ligands exist after QPLD in comparison to standard Glide-XP docking

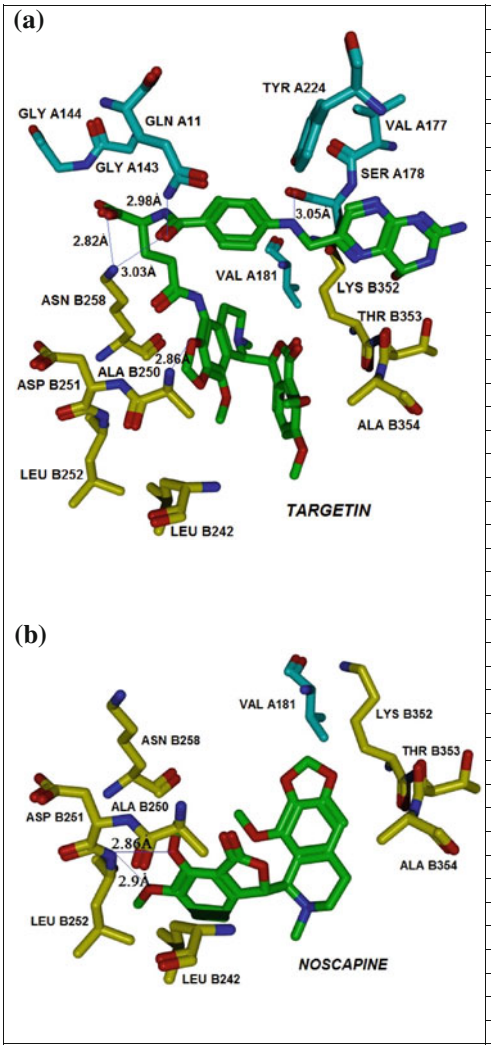

Tubulin	Targetin	Distance (Å)
ALA B 354 CB	O9	1.610
THR B 353 CA	C4*	2.192
LYS B 352 CD	N5*	2.615
MET B 259 CE	C3''	1.545
ASN B 258 ND2	O8'', O19*	1.689
ALA B 256 CB	C4''	3.863
LEU B 255 CD2	C5''	1.507
LYS B 254 CD	O7''	1.164
LEU B 252 CD2	C9'	3.007
ASP B 251 C	C12'	2.063
ALA B 250 N	C2'	1.005
ASN B 249 CG	C2'	3.093
LEU B 248 CD1	O3'	0.867
GLN B 247 CD	C12'	2.496
LEU B 242 CD1	C6	3.308
CYS B 241 CA	C5	1.475
TYR A 224 CZ	C7*	2.628
VAL A 181 CA	C11*	2.409
ALA A 180 CB	C13*	2.911
SER A 178 O	N10*	1.762
VAL A 177 CB	N8*	3.313
GLY A 144 CA	C1''	3.274
GLY A 143 CA	C1''	3.896
GLN A 11 NE2	N18*	2.439
Tubulin	Noscapine	Distance (Å)
ALA B 354 CB	N6'	1.949
THR B 353 CA	C9'	3.165
LYS B 352 CD	C2'	2.426
MET B 259 CE	C12	3.588
ASN B 258 CB	C12	3.470
ALA B 256 CB	C4	2.713
LEU B 255 CD2	C5	1.315
LYS B 254 CD	C5	1.609
LEU B 252 N	O9,O10	0.734
ASP B 251 C	C12	2.427
ALA B 250 CA	C12	1.462
ASN B 249 CG	C12	3.793
LEU B 248 CD1	C12	2.639
GLN B 247 CD	C12	3.496
LEU B 242 CD1	C6	3.058
CYS B 241 CA	C7	1.372
VAL A 177 CB	C2'	3.455
SER A 178 CA	C2'	3.823

Fig. 5 Three-dimensional representations of the mode of interactions observed between: **a** tubulin and Targetin, **b** tubulin and noscapine. Only the amino acids within 4.0 Å from the docked ligand are shown in the figure. **a** Targetin interacts with the residues of tubulin with 5 hydrogen bonds (*lines*) and **b** the interaction of noscapine with the residues of tubulin that involve only two hydrogen bonds (*line*). Targetin and noscapine interacts partially with both α-tubulin (*blue carbons*) and β-tubulin (*deep yellow carbons*). Some amino acids (ASN A101, ALA A180, CYS B241, GLN B244, LEU B248, ASN B246, LEU B255, ALA B256, MET B259) that overlay above the ligands have been removed to improve the clarity in figures. The different energy parameters are: columbic interaction (E_{coul}), van der Waal interaction (E_{vdw}) and hydrogen bonding interaction (E_{Hbond})

discovery. Accurate calculation of atomic partial charges of a ligand in the field of the receptor would result in improved docking results. Therefore, we refined the binding poses of both the ligands from Glide XP docking (which relies on the default force field charges) using QPLD after optimizing the atomic charges by QM/MM calculation. QPLD provided a more precise binding pose of Targetin and noscapine with improved docking score of −11.295 and −4.752 kcal/mol. The top scoring poses returned by QPLD were analyzed using Maestro graphical interface. Both ligands docked well at the interface between α- and β-tubulin (Fig. 2a–d). However, the bulky folate moiety of Targetin extends laterally through the inter-protofilament interface towards lumen of the microtubule (Fig. 2c). Targetin is also well accommodated inside the binding cavity due to availability of enough space. The folate moiety is well placed at the distal part of the binding cavity, whereas the conjugated noscapine is buried inside the binding cavity and overlaid with the lead compound, noscapine (Fig. 3). The existence of significant changes in partial charges of both ligands (Fig. 4) after QPLD in comparison to standard Glide-XP docking have significantly improved the binding poses of both the ligands with tubulin. The binding mode of Targetin and noscapine involves interactions with both α- and β-tubulin (Fig. 5). The folate moiety of Targetin is extended laterally to interact with the α-tubulin, whereas the conjugated noscapine is biased to interact with β-tubulin (Fig. 5a). Five hydrogen bonds are involved in the binding of Targetin with tubulin. The nitrogen atoms (N10* and N18*) of folate moiety form H-bonds with the carbonyl oxygen of SER 178 (bond length 3.05 Å, and GLN 11 (bond length 2.98 Å) of α-tubulin, the oxygen atoms (O8″ and O19*) of folate moiety form H-bonds (bond length 2.82 and 3.03 Å) with side chain nitrogen (ND2) of ASN 258 of β-tubulin, whereas the oxygen atom (O1′) of isoquinoline ring of the conjugated noscapine is involved in H-bonding (bond length 2.86 Å) with backbone nitrogen of ALA 250 of β-tubulin. In case of the lead molecule, noscapine, both the oxygen atoms (O9 and O10) of dimethoxy groups in the isobenzofuranone ring involve H-bonding interactions (bond length 2.86 and 2.9 Å) with LEU 252

of β-tubulin. Furthermore, both ligands showed desirable hydrophobic interactions with the hydrophobic residues within the binding cavity as mentioned in Fig. 5. The energy decomposition of binding site amino acids (e.g. columbic, van der Waals, and hydrogen bond energy) involved in the interaction of Targetin and noscapine is included in Fig. 6. The favourable H-bonding, columbic, and hydrophobic interaction energies make both compounds active and selective for tubulin.

In order to maximize the utility of computer-aided drug discovery methods the binding affinities of both ligands with tubulin were calculated by molecular mechanics energy minimization of QPLD docked complexes using Prime MM-GBSA and Liasion. Various descriptors extracted from the structural information on ligand-receptor complex have added valuable information in our in silico evaluation of the ligands for a reliable binding-affinity. Concisely, various energy components that contribute to the binding energy such as free energy, solvation energy, and surface area energy were calculated for the complex holoenzyme, apoenzyme, and free ligand. Binding free energy (ΔG_{bind}) was calculated as the sum of difference between energy of complex holoenzyme and sum of energy of apoenzyme and free ligand. The ΔG_{bind} energy calculated based on Prime MM-GBSA for Targetin and noscapine was −221.012 and −30.441 kcal/mol (Table 3). The higher binding energy of Targetin in comparison to noscapine was due to largest contribution of electrostatic, van der Waal, and ligand strain energy (Table 3), which is expected due to the substitution of folate group that interact favourably with a binding cavity lined with hydrophobic and hydrophilic amino acids. The large value of cavity energy for Targetin signifies the fact that binding is largely driven by the ligand's ability to bury itself in the binding cavity as evident from the high value of ligand strain energy (49.82 kcal/mol) in contrast to noscapine (11.65 kcal/mol). The energy of Targetin in free form is −116.86 kcal/mol whereas in complex with receptor is −67.04 kcal/mol. Hence, maximum energy is lost (represented as ligand strain energy) due to favourable interaction of Targetin with the receptor. There are subtle interactions between folate moiety at the distal part of the binding cavity as well as the conjugated noscapine at the bottom of the binding cavity.

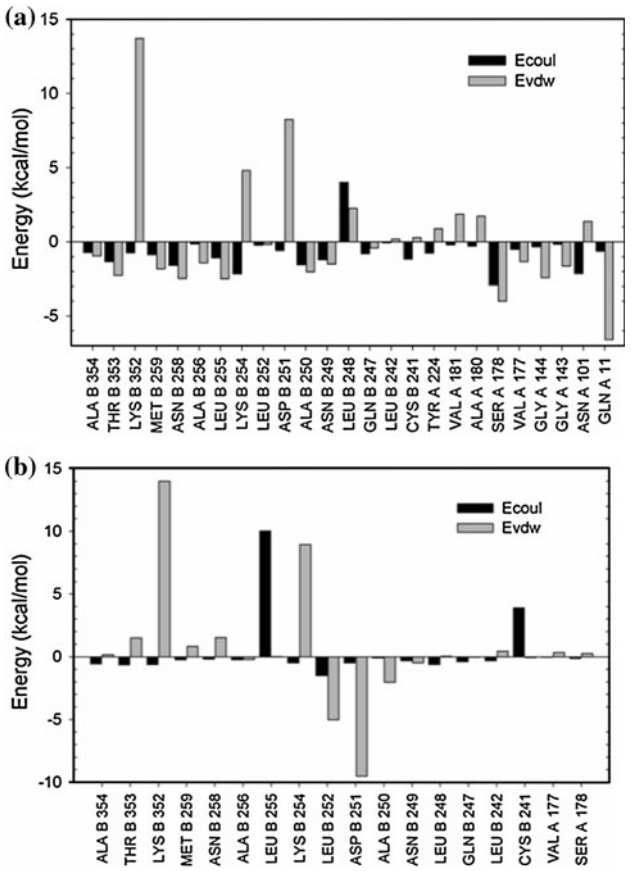

Fig. 6 Energy contribution (Ecoul: Columbic interaction and E_{vdw} vander Waals) of binding site amino acids with **a** Targetin, and **b** Noscapine

Chemical synthesis

Inspired by molecular modelling evaluation of Targetin as a potent molecule that could retain binding with tubulin, we sought to experimentally test this idea. To do this, we first synthesized Targetin by coupling folic acid activated ester, folate-NHS to 9-amino-noscapine. The γ-carboxylic group of folic acid was not reactive enough to participate in the coupling reaction and hence was activated using *N*-hydroxysuccinimide (NHS) and dicyclohexylcarbodiimide

Table 3 Calculated energies and estimated binding free energy (ΔG_{bind}) of Targetin and noscapine with tubulin based on molecular mechanics energy minimizations

Ligand	Prime MM-GBSA ΔG_{bind} (kcal/mol)	Prime MM-GBSA Ligand strain energy (kcal/mol)	$\langle U_{vdw} \rangle$ (kcal/mol)	$\langle U_{ele} \rangle$ (kcal/mol)	$\langle U_{cav} \rangle$ (kcal/mol)
Targetin	−221.01	49.82	−73.29	−148.46	11.13
Noscapine	−30.44	11.65	−54.46	50.22	2.29

$\langle U_{vdw} \rangle$, $\langle U_{ele} \rangle$, and, $\langle U_{cav} \rangle$ energy terms represents the ensemble average energy terms calculated as the difference between bound and free state of ligands and their environments. The various energy parameters are: *vdw* van der Waals energy; *ele* electrostatic energy and *cav* cavity energy

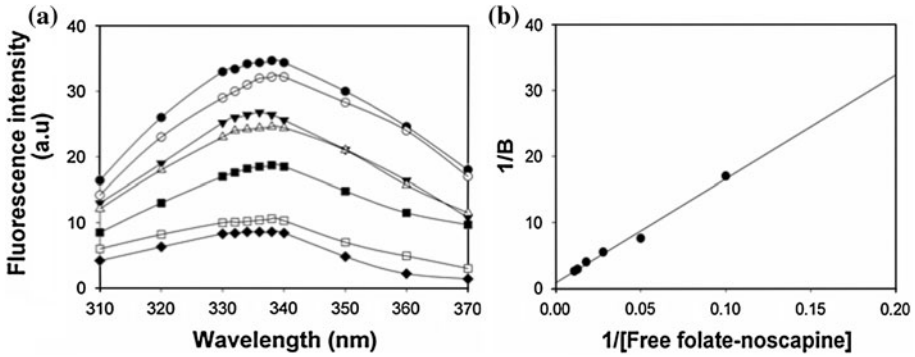

Fig. 7 Binding of Targetin to tubulin as measured by fluorescence quenching of tubulin. **a** Quenching of tubulin fluorescence emission by Targetin in a concentration-dependent manner (control 0 μM (*filled circle*), 10 μM (*open circle*), 20 μM (*inverted filled triangle*), 30 μM (*open triangle*), 50 μM (*filled square*), 75 μ M (*open square*) and 100 μM (*filled diamond*). **b** Double-reciprocal plot showing a dissociation constant (K_d) of 149 ± 3 μM for Targetin binding to tubulin

(DCC) as coupling reagent in DMSO to produce NHS-folate which was then reacted with 9-amino-noscapine. Followed by the successful synthesis of Targetin in good yield (72%) we evaluated experimentally the binding affinity of Targetin with tubulin in vitro, interference with tubulin polymerization, impact on microtubule dynamics, and effects on cancer cell growth as follows.

Biological studies

Effects of Targetin on tubulin binding

Noscapine was previously found to bind tubulin with a dissociation constant (K_d) of 152 ± 1 μM [20]. To test if Targetin also retains the tubulin-binding property of noscapine, we have used the standard tubulin-binding assay (fluorescence quenching titration) [12, 20] in presence of different concentrations of Targetin. We found that Targetin binds tubulin in a concentration-dependent manner (Fig. 7a, as evident from the fluorescence quenching) with a dissociation constant of 149 ± 3.0 μM (Fig. 7b). This result revealed that Targetin retains the tubulin binding property of noscapine. The K_d value of 152 ± 1 μM for noscapine in these experiments is ~8% off from the value of 144 ± 2.8 μM reported by Zhou et al. [35]. This could be due to different experimental conditions in these studies or the variability due to the well known time dependent decay of tubulin during the course of the experiment. Therefore, the minor differences in the K_d value of Targetin binding to tubulin (149.3 ± 3 μM) cannot be taken to be significantly different from that of noscapine. Nevertheless, because Targetin is a noscapinoid designed to be preferentially taken up by FRα over-expressing cancer cells, it is expected to have much higher biological activity compared to noscapine. The superiority of Targetin in comparison to other potent derivatives such as 9-nitro, 9-bromo and 9-amino derivatives of noscapine (with much lower K_d value) is by virtue of the built in folate moiety in Targetin, it will concentrate intracellularly to a much higher concentrations than free noscapine. Therefore, although noscapine and Targetin share roughly equal K_d values, because of the FRα-facilitated intracellular uptake Targetin concentration in FRα over-expressing cancer cells will be much higher than of noscapine uptake, which is not targeted more specifically to cancer cells.

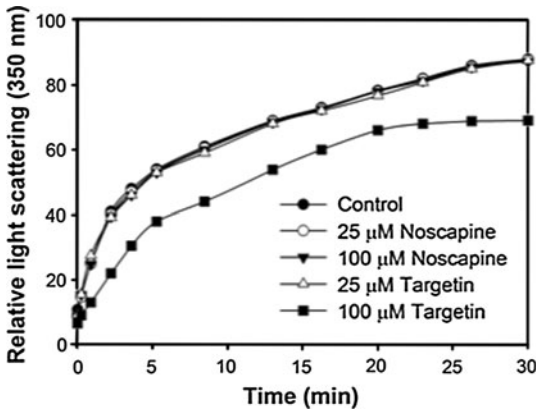

Fig. 8 Effects of noscapine and Targetin on the assembly of tubulin into microtubules in vitro at two concentrations: lower (25 μM) and higher (100 μM). An equivalent amount of the solvent DMSO was used as a control

Effects of Targetin on the assembly of tubulin subunits

We have shown previously that noscapine binds tubulin stoichiometrically and suppresses microtubule dynamics with little effect on bulk microtubule polymer mass and blocks cell cycle progression by the induction of mitotic index [11, 12]. Tubulin assembly into microtubules is typically measured by following changes in turbidity produced upon tubulin polymerization. This analysis revealed that both noscapine and Targetin did not inhibit tubulin polymerization at 25 μM concentration. However, a

fourfold concentration of Targetin (100 μM) inhibited the rate and extent of tubulin polymerization by ~17% (Fig. 8). No evidence of aberrant twisted oligomeric sheets or rings as evident in colchicine induced MT-depolymerization [36] was obtained. Noscapine allows primarily the assembly of normal microtubule lattice as described previously by electron microscopy studies [10].

Effects of Targetin on microtubule dynamic instability in vivo

To determine if Targetin affects microtubule dynamics in living cells, we followed life histories of microtubule plus ends in Targetin-treated cells (transfected with GFP-tagged-α-tubulin) by video microscopy. We have shown previously that in control cells (treated with the vehicle solution DMSO alone), microtubules alternated between phases of growth and shortening, and also spent a small fraction of time in an attenuated state, neither growing nor shortening to a detectable extent [37]. The mean growth rate in the absence of Targetin was 9.15 μm/min, and addition of 5 μM Targetin reduced the growth rate to 8.72 μm/min. Even at a high concentration of 10 μM, targetin reduced the mean growing rate by only 21.86%. Similar to its effects on microtubule growth, Targetin also affected, although modestly, the rate and extent of microtubule shortening. For example, in the presence of 5 and 10 μM Targetin, the shortening rate was reduced by 2.16 and 17.61%, respectively (Fig. 9). In addition, Targetin reduced the percentage of time microtubules spent in the growing and shortening phase (Fig. 9). Microtubules, both in vitro and in living cells, spend a considerable time in an attenuated (pause) state at or near steady state [11]. Strikingly, Targetin increased the percentage of time that the microtubules spent in the attenuated state (Fig. 9). For example, in the presence of 10 μM Targetin, microtubules spent 44.8% of time in the attenuated state, which is increased by 106% when compared to that in the absence of Targetin. The transition frequencies among the growing, shortening, and attenuated states are considered to be important in the regulation of microtubule dynamics [38, 39]. Targetin strongly decreased the catastrophe frequency and increased the rescue frequency (Fig. 9). Dynamicity is a parameter that reflects the overall dynamics of the microtubules (the total detectable tubulin dimer addition and loss at a microtubule end) [11]. As shown in Fig. 9, Targetin (5 and 10 μM) suppressed microtubule dynamicity by 13.62 and 58.4%, respectively. We conclude from these data that Targetin treatment prevents the number of dynamic events in the life history of a microtubule without affecting its long-term existence.

Effect of Targetin on cancer cell growth

We evaluated the ability of Targetin to inhibit cellular proliferation of a variety of cancer cell types using the sulforhodamine B assay (Fig. 10). Our results showed that lung (A549), colon (HCT116), prostate (DU145), breast (T47D) and ovarian (SKOV3 and 1A9) cancer cells were all more sensitive to Targetin compared with noscapine (IC_{50} in the

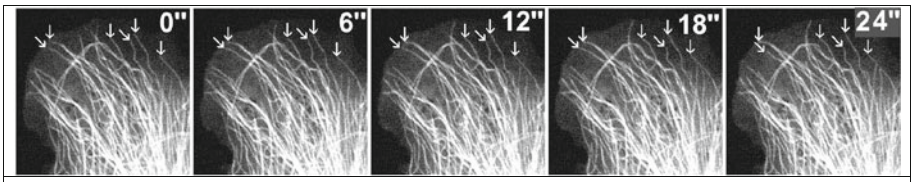

Dynamic parameters	Targetin concentration (μM)		
	0	5	10
Rate (μm/min)			
Growing	9.15 ± 2.72	8.72 ± 1.32	7.15 ± 0.56
Shortening	12.04 ± 2.81	11.78 ± 1.21	9.92 ± 1.25
Percentage of total time			
Growing	41.8	35.2	24.3
Shortening	36.3	28.5	20.1
Attenuation	21.8	32.5	44.8
Transition frequency (sec $^{-1}$)			
Catastrophe	0.086 ± 0.02	0.079 ± 0.07	0.072 ± 0.05
Rescue	0.077 ± 0.01	0.07 ± 0.012	0.059 ± 0.019
Dynamicity (μm/min)	6.61 ± 2.36	4.52 ± 1.21	2.75 ± 1.05
Average pause (sec)	8.16 ± 2.42	10.25 ± 1.25	14.52 ± 2.36

Fig. 9 Targetin treatment suppresses microtubule dynamics and increases the average time cellular microtubules remain active (pause duration). Although all of the microtubule dynamic instability show clear quantitative inhibition, the most striking is the increase in the duration of time that microtubule plus ends spend in an attenuated state—and increase from 21.8 s at 0 μM to 44.8 at 10 μM. The quantitative data tabulated here were collected from images such as displayed at the top panel. The relatively fixed position of the plus ends of several microtubules (*arrows*) over a 24 min time period strikingly underscores the increased attenuation in the dynamics of microtubules by Targetin

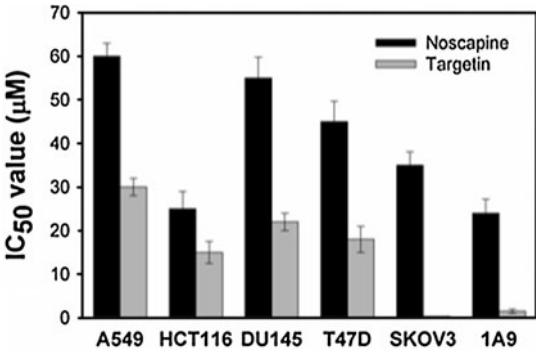

Fig. 10 IC_{50} (a drug concentration required to achieve a 50% inhibition of cellular proliferation) of noscapine (*black bars*) and Targetin (*grey bars*) for various cancer cell types. All the cancer cells used in the assay: lung (A549), colon (HCT116), prostate (DU145), breast (T47D) and ovarian (SKOV3 and 1A9) were more sensitive to Targetin compared with noscapine (IC_{50} in the range of 0.3–30 μM). Particularly striking are the results (IC_{50} 0.3 and 1.5 μM) in both of the ovarian cancer cells (SKOV3 and 1A9) used. These ovarian cancer cell types are known to overexpress folate receptor alpha (FRα) on their surfaces

range of 0.3–30 μM). Of particular note here is that both of the ovarian cancer types tested (SKOV3 and 1A9) were significantly much more sensitive (IC_{50} 0.3 and 1.5 μM) to Targetin. This is perhaps due to their well known overexpression profile of folate receptor alfa (FRα) [40].

Conclusions

Using in silico methodologies, we have been able to design a folate-noscapine analogue, Targetin that retains the activity of noscapine. It also well accommodated within the binding cavity. The in silico results inspired us to chemically synthesize Tagetin, test its tubulin interactions, and evaluate anti-cancer property. Targetin more specifically targeted to aggressive cancer cells that over expressed folate receptor. Taken together our study provides a proof-of-concept for the rational design of specific tumour-targeting drugs based upon the lead molecule noscapine.

Acknowledgments We thank Dr. Dulal panda, IIT Bombay, India, for his support and sharing technical details of Targetin-tubulin interactions and microtubule polymerization assays. Grant supports: NIH grants CA-095317-01A2 (H.C. Joshi) and BOYSCAST fellowship (SR/BY/L-37/09; Department of Science and Technology, Government of India) to Pradeep K. Naik.

References

1. Jordan MA, Wilson L (1999) The use and action of drugs in analyzing mitosis. Methods Cell Biol 61:267–295
2. Fuchs DA, Johnson RK (1978) Cytologic evidence that taxol, an antineoplastic agent from *Taxus brevifolia*, acts as a mitotic spindle poison. Cancer Treat Rep 62:1219–1222
3. Jordan MA, Toso RJ, Thrower D, Wilson L (1993) Mechanism of mitotic block and inhibition of cell proliferation by taxol at low concentrations. Proc Natl Acad Sci USA 90:9552–9556
4. Reider C, Schultz A, Cole R, Sluder G (1994) Anaphase onset in vertebrate somatic cells is controlled by a checkpoint that monitors sister kinetochore attachment to the spindle. J Cell Biol 127:1302–1310
5. Mathe G, Misset JL, De Vassal F, Gouveia J, Hayat M, Machover D, Belpomme D, Pico JL, Schwarzenberg L, Ribaud P, Musset M, Jasmin C, De Luca L (1978) Phase II clinical trial with vindesine for remission induction in acute leukemia, blastic crisis of chronic myeloid leukemia, lymphosarcoma, and hodgkin's disease: absence of cross-resistance with vincristine. Cancer Treat Rep 62:805–809
6. Antoine EC, Rixe O, Auclerc G, Weil M, Khayat D (1997) Docetaxel: a review of its role in breast cancer treatment. Am J Clin Oncol 20:429–432
7. Chang AY, Kim K, Glick J, Anderson T, Karp D, Johnson D (1993) Phase II study of taxol, merbarone, and piroxantrone in stage IV non-small-cell lung cancer. J Natl Cancer Inst 85:346–347
8. McGovren JP (1994) Pharmacologic considerations in cancer chemotherapy. Cancer chemotherapy handbook. Appleton & Lange, Norwalk, pp 15–34
9. Calvaletti G, Tredici G, Braga M, Tazzari S (1995) Experimental peripheral neuropathy induced in adult rats by repeated intraperitoneal administration of taxol. Exper Neurol 133:64–72
10. Ye K, Ke Y, Keshava N, Shanks J, Kapp IA, Tekmal RR, Petros J, Joshi HC (1998) Opium alkaloid noscapine is an antitumor agent that arrests metaphase and induces apoptosis in dividing cells. Proc Natl Acad Sci USA 95:2280–2286
11. Landen JW, Lang R, McMahon SJ, Rusan NM, Yvon AM, Adams AW, Sorcinelli MD, Campbell R, Bonaccorsi P, Ansel JC, Archer DR, Wadsworth P, Armstrong CA, Joshi HC (2002) Noscapine alters microtubule dynamics in living cells and inhibits the progression of melanoma. Cancer Res 62:4109–4114
12. Zhou J, Panda D, Landen JW, Wilson L, Joshi HC (2002) Minor alteration of microtubule dynamics causes loss of tension across kinetochore pairs and activates the spindle checkpoint. J Biol Chem 277:17200–17208
13. Zhou J, Gupta K, Yao J, Ye K, Panda D, Giannakakou P, Joshi HC (2002) Paclitaxel-resistant human ovarian cancer cells undergo c-Jun NH2-terminal kinase-mediated apoptosis in response to noscapine. J Biol Chem 277:39777–39785
14. Dahlstrom B, Mellstrand T, Lofdahl CG, Johansson M (1982) Pharmakokinetic properties of noscapine. Eur J Clin Pharmacol 22:535–539
15. Karlsson MO, Dahlstrom B, Eckernas SA, Johansson M, Alm AT (1990) Pharmacokinetics of oral noscapine. Eur J Clin Pharmacol 39:275–279
16. Aneja R, Dhiman N, Idnani J, Awasthi A, Arora SK, Chandra R, Joshi HC (2007) Preclinical pharmacokinetics and bioavailability of noscapine, a tubulin-binding anticancer agent. Cancer Chemother Pharmacol 60(6):831–839
17. Ke Y, Ye K, Grossniklaus HE, Archer DR, Joshi HC, Kapp JA (2000) Noscapine inhibits tumor growth with little toxicity to normal tissues or inhibition of immune responses. Cancer Immunol Immunother 49:217–225
18. Aneja R, Vangapandu SN, Lopus M, Chandra R, Panda D, Joshi HC (2006) Development of a novel nitro-derivative of noscapine for the potential treatment of drug-resistant ovarian cancer and T-cell lymphoma. Mol Pharmacol 69:1801–1809
19. Aneja R, Vangapandu SN, Lopus M, Viswesarappa VG, Dhiman N, Verma A, Chandra R, Panda D, Joshi HC (2006) Synthesis of microtubule-interfering halogenated noscapine analogs that perturb mitosis in cancer cells followed by cell death. Biochem Pharmacol 72:415–426

20. Naik PK, Chatterji BP, Vangapandu SN, Aneja R, Chandra R, Kanteveri S, Joshi HC (2011) Rational design, synthesis and biological evaluations of amino-noscapine: a high affinity tubulin-binding noscapinoid. J Comput Aided Drug Des 25(5): 443–454
21. Naik PK, Santoshi S, Rai A, Joshi HC (2011) Molecular modelling and competition binding study of Br- noscapine and colchicine provide insight into noscapinoid-tubulin binding site. J Mol Graph Model 29:947–955
22. Parker N, Turk MJ, Westrick E, Lewis JD, Low PS, Leamon CP (2005) Folate receptor expression in carcinomas and normal tissues determined by a quantitative radioligand binding assay. Anal Biochem 338:284–293
23. Ross JF, Chaudhuri PK, Ratnam M (1994) Differential regulation of folate receptor isoforms in normal and malignant tissues in vivo and in established cell lines. Physiologic and clinical implications. Cancer 73:2432–2443
24. Ravelli RB, Gigant B, Curmi PA, Jourdain I, Lachkar S, Sobel A, Knossow M (2004) Insight into tubulin regulation from a complex with colchicines and a stathmin-like domain. Nature 428: 198–202
25. Friesner RA, Banks JL, Murphy RB, Halgren TA, Klicic JJ, Mainz DT, Repasky MP, Knoll EH, Shelley M, Perry JK, Shaw DE, Francis P, Shenkin PS (2004) Glide: a new approach for rapid, accurate docking and scoring. 1. Method and assessment of docking accuracy. J Med Chem 47:1739–1749
26. Halgren TA, Murphy RB, Friesner RA, Beard HS, Frye LL, Pollard WT, Banks JL (2004) Glide: a new approach for rapid, accurate docking and scoring. 2. Enrichment factors in database screening. J Med Chem 47:1750–1759
27. Eldridge MD, Murray CW, Auton TR, Paolini GV, Mee RP (1997) Empirical scoring functions: I. The development of a fast empirical scoring function to estimate the binding affinity of ligands in receptor complexes. J Comput Aided Mol Des 11:425–445
28. Bag S, Tawari NR, Degani MD, Queener SF (2010) Design, synthesis, biological evaluation and computational investigation of novel inhibitors of dihydrofolate reductase of opportunistic pathogens. Bioorg Med Chem 18:3187–3197
29. Alam MA, Naik PK (2009) Molecular modelling evaluations of the cytotoxic activity of podophyllotoxin analogues. J Comput Aided Mol Des 23:209–225
30. Zhou R, Frienser RA, Ghosh A, Rizzo RC, Jorgensen WL, Levy RM (2001) New linear interaction method for binding affinity calculations using a continuum solvent model. J Phys Chem B 105:10388–10397
31. Alam MA, Naik PK (2009) Applying linear interaction energy method for binding affinity calculations of podophyllotoxin analogues with tubulin using continuum solvent model and prediction of cytotoxic activity. J Mol Graph Model 27:930–943
32. Guo W, Lee T, Sudimack J, Lee R (2000) Receptor-specific delivery of liposomes via folate-PEG-chol. J Liposome Res 10(2&3):179–195
33. Hamel E, Lin CM (1981) Glutamate-induced polymerization of tubulin: characteristics of the reaction and application to the large-scale purification of tubulin. Arch Biochem Biophys 209:29–40
34. Panda D, Chakrabarti G, Hudson J, Pigg K, Miller HP, Wilson L, Himes RH (2000) Suppression of microtubule dynamic instability and treadmilling by deuterium oxide. Biochemistry 39:5075–5081
35. Zhou J, Gupta K, Aggarwal S, Aneja R, Chandra R, Panda D, Joshi HC (2003) Brominated derivatives of noscapine are potent microtubule-interfering agents that perturb mitosis and inhibit cell proliferation. Mol Pharmacol 63:799–807
36. Andreu JM, Timasheff SN (1982) Tubulin bound to colchicine forms polymers different from microtubules. Proc Natl Acad Sci USA 79:6753–6756
37. Aneja R, Asress S, Dhiman N, Awasthi A, Rida PCG, Arora SK, Zhou J, Glass JD, Joshi HC (2010) Non-toxic melanoma therapy by a novel tubulin-binding agent. Int J Cancer 126:256–265
38. Belmont LD, Hyman AA, Sawin KE, Mitchison TJ (1990) Real-time visualization of cell cycle-dependent changes in microtubule dynamics in cytoplasmic extracts. Cell 62:579–589
39. Gliksman NR, Skibbens RV, Salmon ED (1993) How the transition frequencies of microtubule dynamic instability (nucleation, catastrophe, and rescue) regulate microtubule dynamics in interphase and mitosis: analysis using a Monte Carlo computer simulation. Mol Biol Cell 4:1035–1050
40. Kalli KR, Oberg AL, Keeney GL, Christianson TJ, Low PS, Knutson KL, Hartmann LC (2008) Folate receptor alpha as a tumor target in epithelial ovarian cancer. Gynecol Oncol 108:619–626